ENGINEERING RESEARCH JOURNAL (ERJ)
Vol. 1, No. 44 April 2020, pp.80-88.
Journal Homepage: erj.bu.edu.eg

Effect of Airfoil Shape on the Aerodynamic performance of a Vertical Axis Wind Turbine

M. R. Rashed [a,b], O. E. Abdellatif [b], M. F. Abd Rabbo [b], E. E. Khalil [c], I. Shahin [b]
[a] Mechanical Engineering Dept., Faculty of Engineering-MTI University, Cairo, Egypt
[b] Mechanical Engineering Dept., Faculty of Engineering at Shoubra-Benha University, Cairo, Egypt
[c] Mechanical Power Engineering Dept., Faculty of Engineering-Cairo University, Giza, Egypt

Abstract
Vertical Axis Wind Turbines (VAWTs), which are one of the most promising wind energy harvesters have started recently to attract more and more attention due to their several advantages, especially in the small-scale wind turbines market. This study employed ANSYS Fluent software to numerically investigate the impact of airfoil profile on the aerodynamic forces generated on the blades of a VAWT. This research employed the NACA four-digit series in order to examine the influence of blade thickness and blade camber. 2D CFD model is employed for this study, the results showed that increasing blade thickness is decreasing the torque and power coefficients. On the other hand, there was an improvement in terms of torque and power coefficients when symmetric airfoil used compared to non-symmetric airfoil.

1. Introduction

Energy is a decisive factor for developing human needs nowadays. Thus, providing a consistent source of energy in a reasonable cost is vital for improving human lifestyle, and increasing economic growth rate globally. Renewable energy resources generally, and wind energy particularly, is a perfect solution for handling the energy crisis [1].

Wind energy harvesters capture the kinetic energy carried by the incoming airflow, to convert it into mechanical energy which could be finally transformed to a useful electrical energy through generators. Wind energy harvesters are typically divided into two main types of wind turbines depends on the orientation of the turbine axis of rotation with respect to the airflow direction, horizontal axis wind turbines (HAWTs) and vertical axis wind turbines (VAWTs). HAWTs is the traditional shape widely used for commercial generation of electricity due to many years of research and development. However, this type of wind turbines is still suffering several difficulties in small-scale markets, due to the unsteady nature of wind condition in terms of speed and direction in urban areas. On the other hand, VAWTs are appropriate for handling such unsteady conditions [2]. VAWTs are classified into two main types based on the driving force, Darrieus type which is based on the lift force, and Savonius type which is based on the drag force. The purpose of this research is to investigate the effect of airfoil shape on the resulting power coefficient of a straight Darrieus VAWT. In this regard, the effect of airfoil shape on the aerodynamic performance of VAWTs has been examined both numerically [3]–[5] and experimentally [5]–[8]. Singh et al. [8], experimented the influence of turbine solidity at various wind velocities on the performance of a three-bladed straight Darrieus VAWT with a non-symmetrical S1210 airfoil. results pointed out that high solidity enhances the power coefficient and the performance of VAWTs generally. The optimal value of the turbine solidity was also figured out for the specific mean wind velocity on spot where the experiment was carried out. Qamar et al. [4], examined the impact of solidity for Darrieus VAWTs and assured Singh et al. [8] conclusion that there is an optimal value of turbine solidity where the performance coefficient approaches the highest value for a specified mean wind velocity. Subramanian et al. [9], analyzed numerically the impact of several NACA airfoils on the aerodynamic performance of VAWTs and concluded that different airfoils react in different ways in accordance with changes in the tip speed ratios; thicker blades behave better at lower tip speed ratios due to the extended time interval of the attached flow, on the other hand, thinner airfoils have an improved performance at high tip speed ratios as they dispel the vortex shedding more rapidly. One of the VAWTs disadvantages is their high turbulence intensity on a turbine's downwind side, which is produced by the upwind side interaction between the turbine blades and freestream wind. Mohamed [10] employed 2D CFD simulations to compare the resulted power coefficient of a straight Darrieus VAWT using symmetric and non-symmetric airfoils and concluded that the use of non-symmetric S-1046 airfoil increased the turbine power output by 26.83% when compared to that of a symmetric NACA airfoil. Mohamed's [10] inferences on the improvement of power coefficient were also confirmed by Sengupta et al. [11] through using non-symmetrical airfoils instead of symmetrical ones at lower wind velocities (4 m/s to 8 m/s). Saeidi et al. [12], explored the impacts of tip speed ratio and solidity on power coefficient for a three-bladed straight Darrieus turbine with a NACA 4415 airfoil. It was realized that the

maximized power coefficient of 0.47 took place at solidity of 0.4 and tip speed ratio of 4. Furthermore, a reduction of 50% in terms of electric power generation cost was spotted at the maximized power coefficient. Ma et al. [13], concentrated on optimizing airfoil shape in order to enhance the power coefficient of a three-bladed VAWT. With the aid of combining the genetic algorithm with CFD simulations, the power coefficient improved nearly by 27%.

2. Numerical Methodologies

2.1. Governing Equations

The numerical simulation is performed with a two-dimensional unsteady turbulent flow system. Governing equations are:

Continuity equation:

$$\nabla \cdot \left(\rho \vec{V}\right) = 0 \tag{1}$$

Momentum equations:

X-momentum equation:

$$\frac{\partial(\rho u)}{\partial t} + \nabla \cdot \left(\rho u \vec{V}\right) = -\frac{\partial p}{\partial x} + \frac{\partial \tau_{xx}}{\partial x} + \frac{\partial \tau_{yx}}{\partial y} \tag{2}$$

Y-momentum equation:

$$\frac{\partial(\rho v)}{\partial t} + \nabla \cdot \left(\rho v \vec{V}\right) = -\frac{\partial p}{\partial y} + \frac{\partial \tau_{xy}}{\partial x} + \frac{\partial \tau_{yy}}{\partial y} \tag{3}$$

2.2. Turbulence modeling

The realizable k—ε turbulence model which has been presented by Shih et al. [14] is employed in the present study. The realizable k—ε turbulence model is proposing transport equation for the turbulent dissipation rate which enhances the features of the model. The realizable k—ε turbulence model offers an outstanding behaviour for flows which involve recirculation, separation, rotation and flow under high level of adverse pressure gradients [15]. furthermore, the realizable k—ε turbulence model presented main modifications more improved than the standard k—ε model where the flow characteristics involve extreme streamline curvature, vortices, and rotation. The transport equations for k and ε in the realizable k—ε model is outlined in the next equations [15]:

$$\frac{\partial}{\partial t}(\rho k) + \frac{\partial}{\partial x_i}\left(\rho k u_j\right) = \frac{\partial}{\partial x_i}\left[\left(\mu + \frac{\mu_t}{\sigma_k}\right)\frac{\partial k}{\partial x_j}\right] + G_k + G_b - \rho\varepsilon - Y_M + S_k \tag{4}$$

and

$$\frac{\partial}{\partial t}(\rho \varepsilon) + \frac{\partial}{\partial x_j}\left(\rho \varepsilon u_j\right) = \frac{\partial}{\partial x_j}\left[\left(\mu + \frac{\mu_t}{\sigma_\varepsilon}\right)\frac{\partial \varepsilon}{\partial x_j}\right] + \rho C_1 S_t - \rho C_2 \frac{\varepsilon^2}{k + \sqrt{\nu\varepsilon}} + C_{1\varepsilon}\frac{\varepsilon}{k} C_{3\varepsilon} G_b + S_t \tag{5}$$

where

$$C_1 = max\left[0.43, \frac{\eta}{\eta + 5}\right] \tag{6}$$

and

$$\eta = S\frac{k}{\varepsilon} \tag{7}$$

2.3. Numerical settings

The flow across the VAWT is modeled employing the finite volume-based commercial CFD software package ANSYS Fluent 19 R1. The incompressible Unsteady Reynolds-Averaged Navier-Stokes (URANS) equations are solved using the double precision coupled pressure-velocity coupling scheme and second order spatial and temporal discretization schemes. These numerical settings are chosen in the wake of several number researches carried out [16]–[19], where the achieved results by means of these settings paved the road to a accepted results with the experimental ones. Symmetry boundary condition was utilized on both the top and bottom sides of the domain, with 10 m/s velocity at inlet side, while the outlet side was set at zero-gauge pressure outlet, as well as the turbulence intensity (TI) value set to be 5% for both inlet and outlet [20]. A no-slip condition is used on the airfoil walls. A domain interface is circumscribed between the rotating cylinder and the fixed domain. The azimuthal increment for the CFD simulations of the turbine set to be 0.5° [21]. Data collecting for the CFD computations is begun after 25 revolutions of the turbine to ensure converged results. The number of iterations per time step is set to be 25 in order to guarantee that all scaled residuals drop below 1×10^5 [21].

2.4. Key performance parameters

The turbine power output is assessed as the non-dimensional power coefficient C_P where,

$$C_P = \lambda C_t \tag{8}$$

where the tip speed ratio λ is described as,

$$\lambda = \frac{\omega R}{V} \tag{9}$$

and ω is the turbine rotational speed, R is the turbine radius, V is the free stream velocity, and the turbine torque C_t is described as,

$$C_t = \frac{T}{0.5\rho A R V^2} \tag{10}$$

2.5. Optimal tip speed ratio

The tip speed ratio (λ) and the turbine solidity (σ) are very important factors for evaluating the performance of wind turbines. Rezaeiha et al. [22] investigated the relation between the aforementioned parameters and the

maximum available power coefficient $(C_{P_{max}})$, as shown in Figure 2-1.

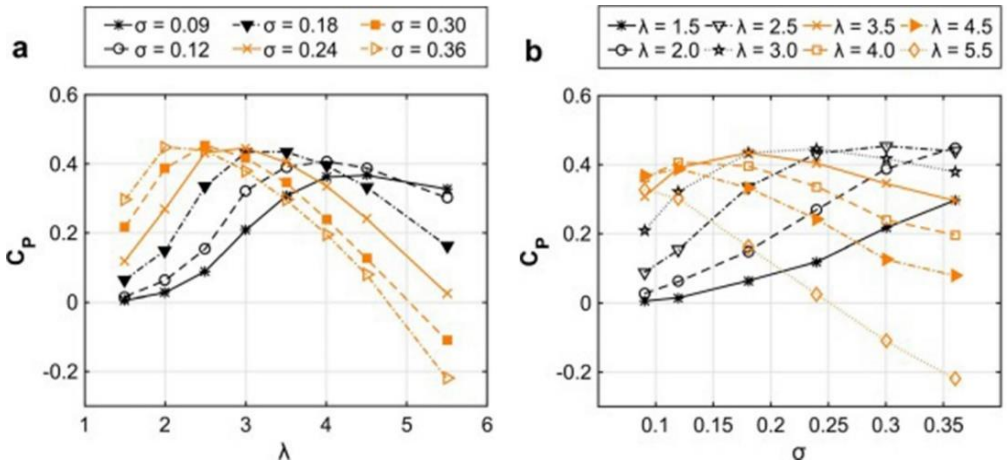

Figure 2-1 Power coefficient versus (a) tip speed ratio and (b) solidity [22]

It was found that the optimal tip speed ratio (λ_{opt}), which the $C_{P_{max}}$ occurs, decreases as the σ increases. Figure 2-2 displays the fitted curve (red curve) through several number of experimental and numerical studies.

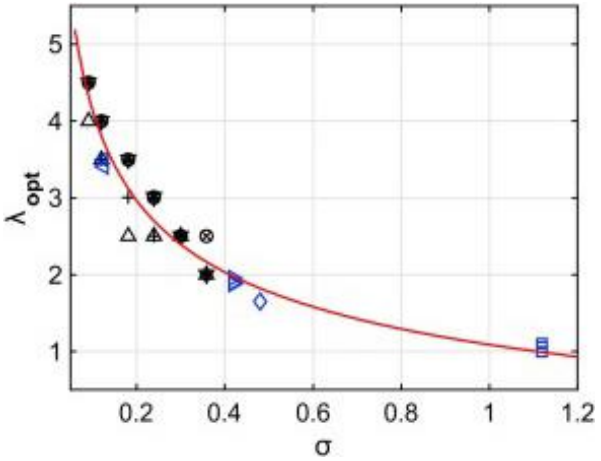

Figure 2-2 Optimal tip speed ratio vs. solidity with a curve fit [22]

Therefore, the λ_{opt} could be estimated for a given σ through the next equation [22]:

$$\lambda_{opt} = 2.693\sigma^{-0.329} - 1.609 \quad (11)$$

Which will lead to estimate the desired turbine rotational velocity (ω) to maximize the output power.

3. Computational Domain and Grid

3.1. Computational domain

In order to simulate the rotation of the VAWT, the computational domain is split up into a rotating cylinder with a diameter of 1.5 times the turbine diameter (rotates in counter clock wise rotational direction) and a fixed domain surrounding the rotating cylinder as shown in Figure 3-1. For the turbine to rotate, a non-conformal interface with sliding grid between the fixed domain and the rotating cylinder was created.

More precisely, the computational domain origin is located at the center of rotating cylinder, while the distance from the cylinder center to the domain inlet is 15 times the turbine diameter and correspondingly the distance from the cylinder center to the domain outlet is 25 times the turbine diameter, whereas the domain width is 20 times the turbine diameter. It is noteworthy that the aforementioned computational domain dimensions was recommended by the research study done by Rezaeiha et al. [23].

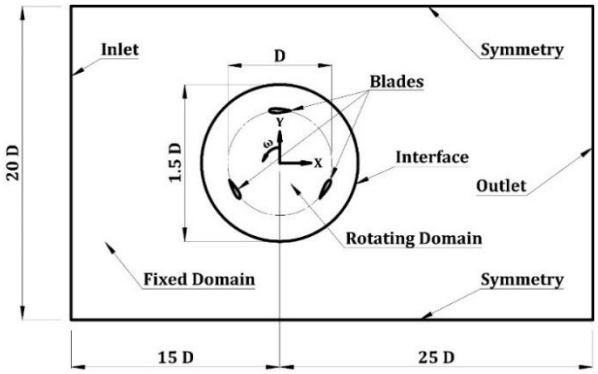

Figure 3-1 Schematic of the two-dimensional computational domain

3.2. Computational grid

For all turbine models employed in the present study the computational grid is created by the using of triangular cells method. The maximum cell skewness in the grid is 0.7 and the minimum orthogonal quality is 0.4. The cell sizing function is employed on the airfoil walls in order to enhance the computational accuracy. The cell size is equal for both sides of the interface between the rotating and fixed domains in order to reduce the numerical errors at this interface. The highest y^+ value is below 6 on the airfoils in order to effectively capture the linear viscous sublayer. The average number of cells through all the studied models is approximately 420,000 cells. Figure 3-2 illustrates the computational grid employed for the present study.

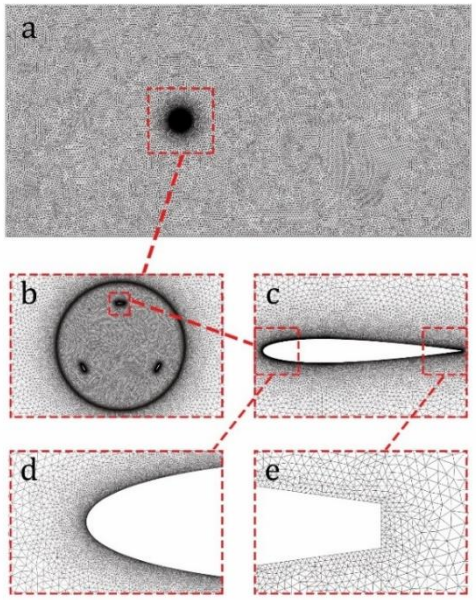

Figure 3-2 Computational Grid: (a) the computational domain; (b) near the rotating cylinder; (c) near the airfoil; (d) near the airfoil leading edge; (e) near the airfoil trailing edge

3.3. Grid sensitivity analysis

The computational grid is one of the most important factors to ensure the accuracy and reliability of the results. Consequently, the best possible grid should be determined to ensure an effective compromise between accuracy of the results and the computational costs in terms of calculation time required. Therefore, four different grids, as presented in Table 3-1, are implemented in the present study.

Table 3-1 Details of the computational grids

Grid name	Number of cells	Maximum y^+ on blades
Grid 1	213,347	21.7
Grid 2	282,455	7.78
Grid 3	340,976	6.56
Grid 4	418,091	6.5

The C_T curves for the turbine versus the azimuthal angle for the above-mentioned grids are shown in Fig. 6. The results of Grid 1 are noticeably higher than those of the other three grids. The results of Grid 2 are slightly better than the ones obtained from Grid 1. Finally, the results of the other two grid sets are quite similar. The relative difference in C_T between

Grid 3 and Grid 4 is less than 2.4%, which is negligible. Based on the calculation accuracy and computational time costs, Grid 3 is chosen in the present study.

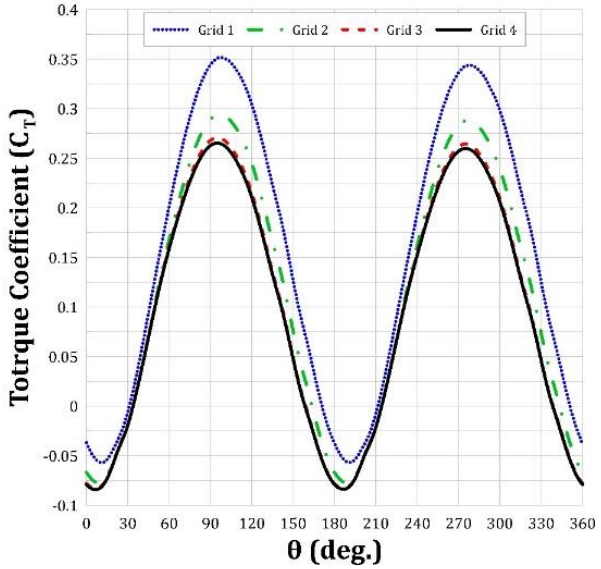

Figure 3-3 Instantaneous C_T of the turbine versus azimuthal angle for four different grids.

4. Model Validation

A VAWT model is used in validation study to guarantee the accuracy and reliability of the CFD simulations, in which the CFD results are compared with the experimental data by Tescione et al. [24]. Table 4-1 shows the different geometrical and operational parameters of the studied validation model.

Table 4-1 Geometrical and operational parameters of validation models

	Validation Model [Tescione et al. 2014]
Turbine diameter $(\boldsymbol{D})$	1000 mm
Turbine height $(\boldsymbol{H})$	1000 mm
Number of blades $(\boldsymbol{N})$	2
Blade profile	NACA 0018
Chord length $(\boldsymbol{c})$	60 mm
Turbine solidity $(\boldsymbol{\sigma})$	0.12
Free stream velocity $(\boldsymbol{V_\infty})$	9.3 m/s
Turbine rotational speed $(\boldsymbol{\omega})$	83.8 rad/s
Tip speed ratio $(\boldsymbol{\lambda})$	4.5

For the validation model, the streamwise normalized velocity at the downstream position, $x/R = 2.0$, along the lateral direction, $-1.5 \leq y/R \leq 1.5$, in the wake of a two-bladed turbine were compared with the experimental data by Tescione et al. [24] as shown in
Figure 4-1.

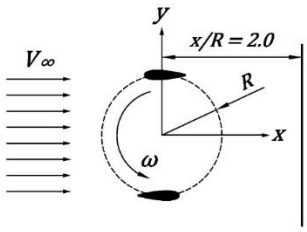

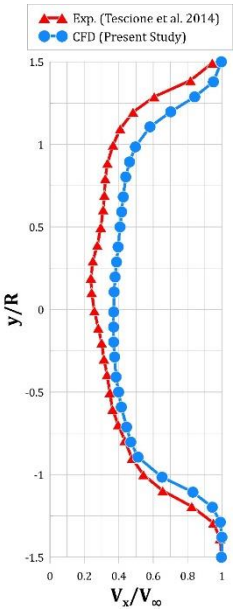

Figure 4-1 Normalized streamwise velocity along the lateral direction at $x/R = 2.0$ downstream in turbine wake at $\lambda = 4.5$

5. Results and Discussion

5.1. Effect of blade thickness

The blade thickness is defined by NACA 00XX in case of symmetric airfoils. The effect of NACA 0012, NACA 0015 and NACA 0018 airfoils will be assessed in this section.

Table 5-1 describes the geometrical and operational parameters of the studied models to investigate the effect of the blade thickness on the turbine performance.

Table 5-1 Geometrical and operational parameters of models (1), (2) and (3)

	Model (1)	**Model (2)**	**Model (3)**
Diameter (D)	1000 mm	1000 mm	1000 mm
Height (H)	1000 mm	1000 mm	1000 mm
Number of blades (N_b)	3	3	3
Blade profile	NACA 0012	NACA 0015	NACA 0018
Chord length (c)	80 mm	80 mm	80 mm
Solidity (σ)	0.24	0.24	0.24
Mounting Position (x_{mp}/c)	0.25	0.25	0.25
Pitch angle (β)	0°	0°	0°
Free stream velocity (V_∞)	10 m/s	10 m/s	10 m/s
Optimal TSR (λ_{opt})	2.70	2.70	2.70
Rotational velocity (ω)	54.0 rad/s	54.0 rad/s	54.0 rad/s

Figure 5-1 shows the torque generated on a single blade for different thicknesses over one complete revolution, it is noticed that during the upwind stage ($0° < \theta < 180°$) that the torque coefficients are almost the same, while during the downwind stage ($180° < \theta < 360°$) a slight deviation started to occur, the deviation increases as the blade thickness increases, and this could be due to the wakes generated by blades in the upwind stage on those located in the downwind stage, which has more significant effect as the thickness increases.

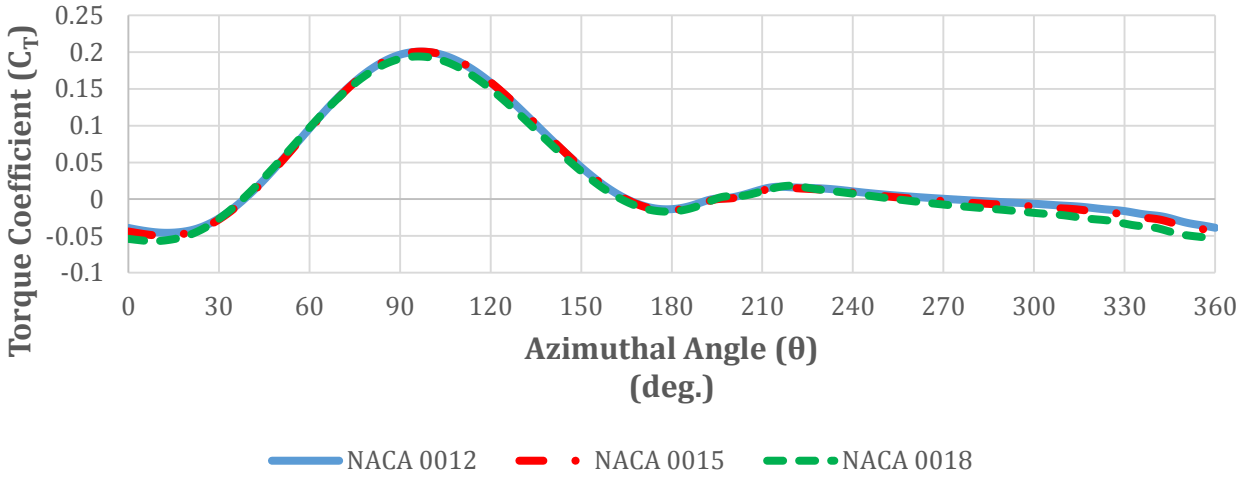

Figure 5-1 Variations of single blade instantaneous torque coefficient versus azimuthal angle for different symmetric airfoils

Figure 5-2 shows the change in torque generated by three-bladed turbine over one complete revolution for symmetric airfoils with different thicknesses, both turbines with NACA 0012 and NACA 0015 airfoil profiles show a slight difference in torque and power produced, while the turbine with NACA 0018 airfoil profile produced a quite remarkable difference. Consequently, airfoil profiles with thickness of 12% of chord length are selected for the present study. However, additional design considerations such as the applied stresses acting on the blade should be taken into account to ensure an efficient and safe operation.

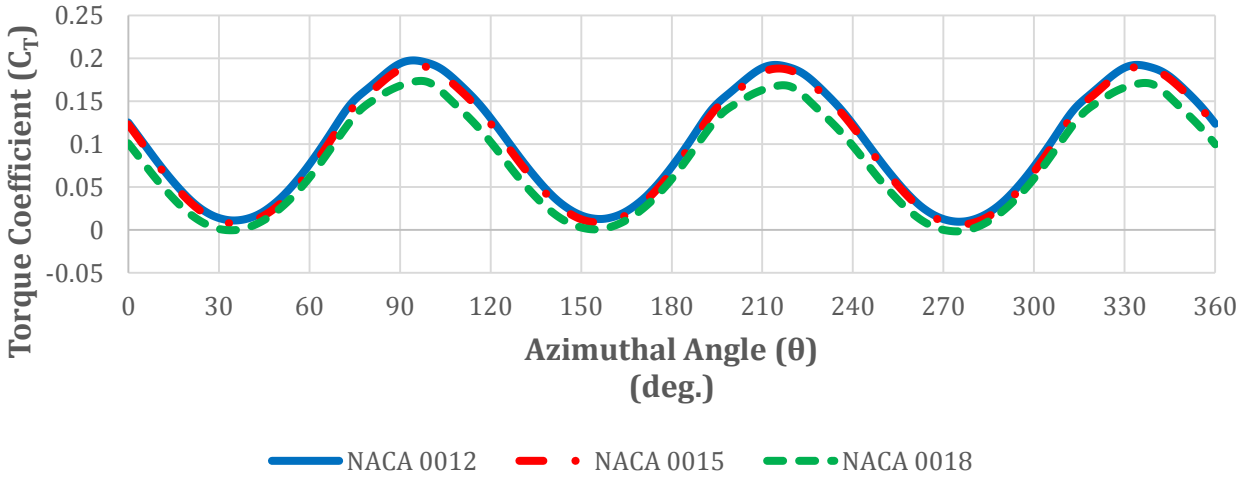

Figure 5-2 Variations of turbine instantaneous torque coefficient versus azimuthal angle for different symmetric airfoils

Table 5-2 compares between the $C_{T_{avg}}$ and $C_{P_{max}}$ generated by turbines with different blade thicknesses (12%, 15% and 18% of chord length). The comparison between the obtained results through this section, highlights that highest $C_{T_{avg}}$ and $C_{P_{max}}$ where generated by the turbine having the thinner blades, and as the blade thickness increases, the time-averaged torque generated decreases, as well as the power produced through this turbine.

Table 5-2 Comparison of torque and power coefficients for models (1), (2) and (3)

	Model (1)	**Model (2)**	**Model (3)**
$C_{T_{avg}}$	0.1015	0.0968	0.0827
$C_{P_{max}}$	0.2744	0.2615	0.2235

5.2. Effect of blade camber

The airfoil camber line exists only in case of non-symmetric airfoils. This section will investigate the effect of symmetric (NACA 0012) and non-symmetric (NACA 4412) airfoil profiles on the VAWTs aerodynamic performance.

Table 5-3 illustrates the geometrical and operational parameters of the studied models to analyze the blade camber effect on the turbine performance.

Table 5-3 Geometrical and operational parameters of models (2) and (6)

	Model (1)	Model (4)
Diameter (D)	1000 mm	1000 mm
Height (H)	1000 mm	1000 mm
Number of blades (N_b)	3	3
Blade profile	NACA 0012	NACA 4412
Chord length (c)	80 mm	80 mm
Solidity (σ)	0.24	0.24
Mounting Position (x_{mp}/c)	0.25	0.25
Pitch angle (β)	0°	0°
Free stream velocity (V_∞)	10 m/s	10 m/s
Optimal TSR (λ_{opt})	2.70	2.70
Rotational velocity (ω)	54.0 rad/s	54.0 rad/s

Figure 5-3 compares between the torque generated by a single blade with two different airfoil profiles, the symmetric NACA 0012 airfoil profile and the non-symmetric NACA 4412 airfoil profile. The investigation shows a higher torque generated by symmetric NACA 0012 airfoil over the upwind stage noticeably compared to that generated by the non-symmetric NACA 4412 airfoil. On the other hand, there was a slight improvement in the torque generated by the non-symmetric NACA 4412 airfoil in the downwind stage compared to that generated by the symmetric NACA 0012 airfoil. However, the overall torque generated in the downwind stage is negligible.

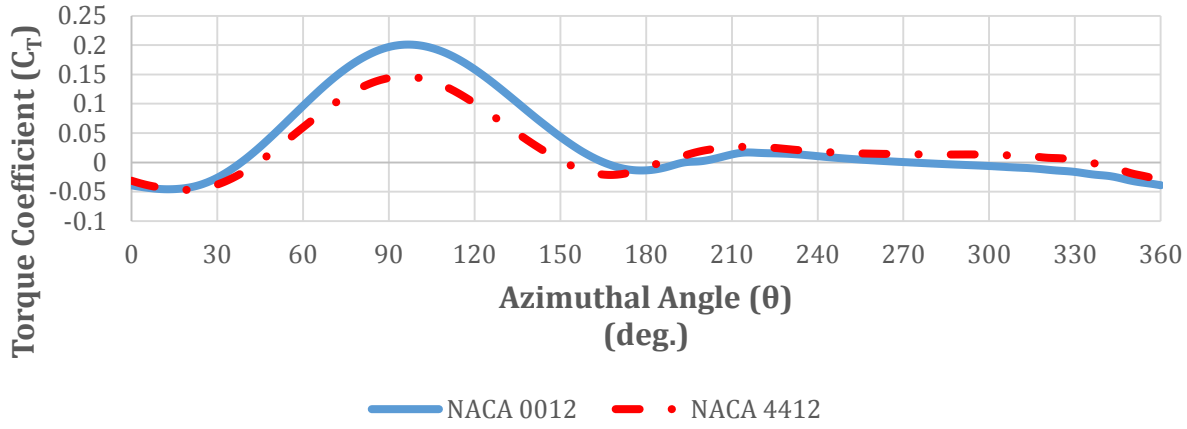

Figure 5-3 Variations of single blade instantaneous torque coefficient versus azimuthal angle for symmetric and non-symmetric airfoils

Figure 5-4 demonstrates the overall torque coefficient generated by a three-bladed (NACA 0012) turbine, and torque coefficient generated by another three-bladed (NACA 4412) turbine. It was quite obvious that the torque generate by the turbine with symmetric airfoil blades was higher than that generated by the turbine with non-symmetric airfoil blades.

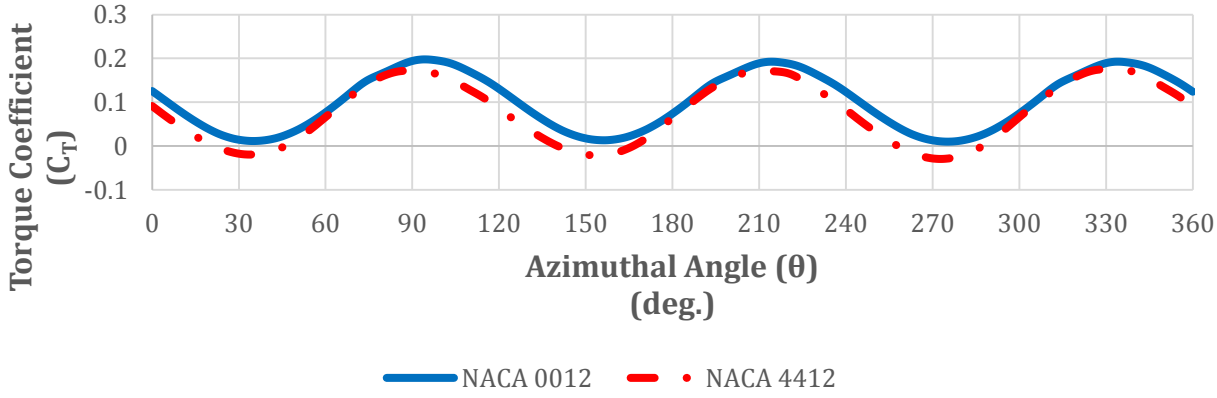

Figure 5-4 Variations of turbine instantaneous torque coefficient versus azimuthal angle for symmetric and non-symmetric airfoils

Table 5-4 compares between the $C_{T_{avg}}$ and $C_{P_{max}}$ generated by turbines with symmetric and non-symmetric airfoil blades. The captured power from the symmetric airfoil bladed turbine is much higher than that captured by the non-symmetric airfoil bladed turbine.

Table 5-4 Comparison of torque and power coefficients for models (1) and (4)

	Model (1)	**Model (4)**
$C_{T_{avg}}$	0.1015	0.0757
$C_{P_{max}}$	0.2744	0.2046

6. Conclusions

The main purpose of the present research is to introduce an improved design for a straight Darrieus rotor for wind energy extraction. Accordingly, the impact of 4 different airfoils is analyzed. Validating the numerical simulations carried out in the present study with experimental work, a precise CFD computations of the unsteady flow surrounding a straight Darrieus rotor have been conducted. The realizable k—ε turbulence model is employed for the CFD simulations to deeply analyze the performance of the turbine.

Blade thickness has been tested over three different thicknesses 12%, 15% and 18% of the chord length. The investigation led to an important finding, that the thinner blade thickness generated higher torque as well as higher power. It could be a result of lower drag produced on the thinner blades.

The use of symmetric a non-symmetric airfoil in the VAWTs design has been studied in this study by employing of the NACA 0012 and NACA 4412 airfoils to examine the effect of blade camber. Both torque and power generated by the turbine employed the NACA 4412 airfoil profile were decreased by 25.4% compared with these generated by the turbine employed the NACA 0012 airfoil profile.

7. References

[1] A. KC, J. Whale, and T. Urmee, "Urban wind conditions and small wind turbines in the built environment: A review," *Renewable Energy*, vol. 131, pp. 268–283, Feb. 2019.

[2] M. Jafari, A. Razavi, and M. Mirhosseini, "Effect of airfoil profile on aerodynamic performance and economic assessment of H-rotor vertical axis wind turbines," *Energy*, vol. 165, no. 6, pp. 792–810, Dec. 2018.

[3] A. Posa, C. M. Parker, M. C. Leftwich, and E. Balaras, "Wake structure of a single vertical axis wind turbine," *International Journal of Heat and Fluid Flow*, vol. 61, pp. 75–84, Oct. 2016.

[4] S. B. Qamar and I. Janajreh, "A comprehensive analysis of solidity for cambered darrieus VAWTs," *International Journal of Hydrogen Energy*, vol. 42, no. 30, pp. 19420–19431, Jul. 2017.

[5] P. Bachant and M. Wosnik, "Characterising the near-wake of a cross-flow turbine," *Journal of Turbulence*, vol. 16, no. 4, pp. 392–410, Apr. 2015.

[6] S. Shamsoddin and F. Porté-Agel, "Large Eddy Simulation of Vertical Axis Wind Turbine Wakes," *Energies*, vol. 7, no. 2, pp. 890–912, Feb. 2014.

[7] S. Shamsoddin and F. Porté-Agel, "A Large-Eddy Simulation Study of Vertical Axis Wind Turbine Wakes in the Atmospheric Boundary Layer," *Energies*, vol. 9, no. 5, p. 366, May 2016.

[8] M. A. Singh, A. Biswas, and R. D. Misra, "Investigation of self-starting and high rotor solidity on the performance of a three S1210 blade H-type Darrieus rotor," *Renewable Energy*, vol. 76, pp. 381–387, Apr. 2015.

[9] A. Subramanian *et al.*, "Effect of airfoil and solidity on performance of small scale vertical axis wind turbine using three dimensional CFD model," *Energy*, vol. 133, pp. 179–190, Aug. 2017.

[10] M. H. Mohamed, "Performance investigation of H-rotor Darrieus turbine with new airfoil shapes," *Energy*, vol. 47, no. 1, pp. 522–530, Nov. 2012.

[11] A. R. Sengupta, A. Biswas, and R. Gupta, "Studies of some high solidity symmetrical and unsymmetrical blade H-Darrieus rotors with respect to starting characteristics, dynamic performances and flow physics in low wind streams," *Renewable Energy*, vol. 93, pp. 536–547, Aug. 2016.

[12] D. Saeidi, A. Sedaghat, P. Alamdari, and A. A. Alemrajabi, "Aerodynamic design and economical evaluation of site specific small vertical axis wind turbines," *Applied Energy*, vol. 101, pp. 765–775, Jan. 2013.

[13] N. Ma *et al.*, "Airfoil optimization to improve power performance of a high-solidity vertical axis wind turbine at a moderate tip speed ratio," *Energy*, vol. 150, pp. 236–252, May 2018.

[14] T.-H. Shih, W. W. Liou, A. Shabbir, Z. Yang, and J. Zhu, "A new k-ϵ eddy viscosity model for high reynolds number turbulent flows," *Computers & Fluids*, vol. 24, no. 3, pp. 227–238, Mar. 1995.

[15] I. Hashem and M. H. Mohamed, "Aerodynamic performance enhancements of H-rotor Darrieus wind turbine," *Energy*, vol. 142, pp. 531–545, Jan. 2018.

[16] A. Bianchini, F. Balduzzi, P. Bachant, G. Ferrara, and L. Ferrari, "Effectiveness of two-dimensional CFD simulations for Darrieus VAWTs: a combined numerical and experimental assessment," *Energy Conversion and Management*, vol. 136, pp. 318–328, Mar. 2017.

[17] A. Bianchini, F. Balduzzi, G. Ferrara, G. Persico, V. Dossena, and L. Ferrari, "A Critical Analysis on Low-Order Simulation Models for Darrieus Vawts: How Much Do They Pertain to the Real Flow?," *Journal of Engineering for*

Gas Turbines and Power, vol. 141, no. 1, Jan. 2019.

[18] F. Balduzzi *et al.*, "Three-Dimensional Aerodynamic Analysis of a Darrieus Wind Turbine Blade Using Computational Fluid Dynamics and Lifting Line Theory," *Journal of Engineering for Gas Turbines and Power*, vol. 140, no. 2, p. 022602, Oct. 2017.

[19] T. Zhang *et al.*, "Winglet design for vertical axis wind turbines based on a design of experiment and CFD approach," *Energy Conversion and Management*, vol. 195, pp. 712–726, Sep. 2019.

[20] A. Rezaeiha, H. Montazeri, and B. Blocken, "On the accuracy of turbulence models for CFD simulations of vertical axis wind turbines," *Energy*, vol. 180, pp. 838–857, Aug. 2019.

[21] Y. Guo, X. Li, L. Sun, Y. Gao, Z. Gao, and L. Chen, "Aerodynamic analysis of a step adjustment method for blade pitch of a VAWT," *Journal of Wind Engineering and Industrial Aerodynamics*, vol. 188, pp. 90–101, May 2019.

[22] A. Rezaeiha, H. Montazeri, and B. Blocken, "Towards optimal aerodynamic design of vertical axis wind turbines: Impact of solidity and number of blades," *Energy*, vol. 165, pp. 1129–1148, Dec. 2018.

[23] A. Rezaeiha, I. Kalkman, and B. Blocken, "CFD simulation of a vertical axis wind turbine operating at a moderate tip speed ratio: Guidelines for minimum domain size and azimuthal increment," *Renewable Energy*, vol. 107, pp. 373–385, Jul. 2017.

[24] G. Tescione, D. Ragni, C. He, C. J. Simão Ferreira, and G. J. W. van Bussel, "Near wake flow analysis of a vertical axis wind turbine by stereoscopic particle image velocimetry," *Renewable Energy*, vol. 70, pp. 47–61, Oct. 2014.